PNAS RESEARCH ARTICLE | BIOCHEMISTRY

Photopharmacological modulation of native CRAC channels using azoboronate photoswitches

Ronald Udasin[a,1], Anwesha Sil[b,1], Elia Zomot[a,1], Hadas Achildiev Cohen[a], Jozafina Haj[c], Nurit Engelmayer[d,e], Shaya Lev[d,e], Alexander M. Binshtok[d,e], Yuval Shaked[c], Michael A. Kienzler[b,2], and Raz Palty[a,2]

Edited by Tullio Pozzan, University of Padova, Padova, Italy; received October 16, 2021; accepted February 22, 2022

Store-operated calcium entry through calcium release–activated calcium (CRAC) channels replenishes intracellular calcium stores and plays a critical role in cellular calcium signaling. CRAC channels are activated by tightly regulated interaction between the endoplasmic reticulum (ER) calcium sensor STIM proteins and plasma membrane (PM) Orai channels. Our current understanding of the role of STIM–Orai-dependent calcium signals under physiologically relevant conditions remains limited in part due to a lack of spatiotemporally precise methods for direct manipulation of endogenous CRAC channels. Here, we report the synthesis and characterization of azoboronate light-operated CRAC channel inhibitors (LOCIs) that allow for a dynamic and fully reversible remote modulation of the function of native CRAC channels using ultraviolet (UV) and visible light. We demonstrate the use of LOCI-1 to modulate gene expression in T lymphocytes, cancer cell seeding at metastatic sites, and pain-related behavior.

CRAC channel | Orai | STIM | azobenzene | photoswitch

Calcium (Ca^{2+}) is an essential and ubiquitous second messenger in cells. Because of its central role in cellular signaling, many proteins, pumps, and ion channels are present in every cell to tightly regulate the spatial and temporal profiles of intracellular calcium. Store-operated calcium entry (SOCE) is a key mechanism by which cells generate calcium signals and maintain calcium homeostasis by replacing calcium lost from the endoplasmic reticulum (ER) with calcium that enters the cytoplasm through plasma membrane (PM) channels (1). Calcium release–activated calcium (CRAC) channels are the prototypical mediators of SOCE in cells (2–4). The two primary components of CRAC channels are stromal interaction molecule (STIM) (5–7) and Orai (8–11) (also referred to as CRACM) proteins. STIM proteins, the ER Ca^{2+} sensors, are activated when the ER is depleted of Ca^{2+} and translocate and aggregate at ER–PM junctions where they bind to the other key component—Orai proteins—which are the CRAC channel pore forming subunits (Fig. 1*A*). Mammalian cells express two STIM isoforms (STIM1 and STIM2) and three Orai isoforms (Orai1–3); however, STIM1 and Orai1 are the best-characterized isoforms of CRAC channels (6–8, 12, 13). They are ubiquitously expressed and have been shown to contribute to diverse cellular functions, including migration, secretion, and gene expression (1). Deficiency in CRAC channel activity due to loss- or gain-of-function mutations in Orai1 or STIM1 is associated with a range of disease states, including skeletal muscle myopathy and severe forms of combined immunodeficiency (14).

Much has been learned about the structure and function of CRAC channels (1). Nonetheless, under physiological settings, the complex choreography of CRAC channel activation results in a miniscule calcium current, which often operates alongside other calcium transport proteins, making its investigation in live cells and tissues a significant challenge. The development of tools that can manipulate CRAC channel function in a cell-type–specific and spatiotemporally precise manner would greatly enhance our understanding of CRAC channel function at the tissue, cellular, and subcellular levels. Indeed, the ability to introduce light sensitivity to the activity of Orai1 channels through optogenetics has been elegantly shown in recent reports (Fig. 1*B*) (15–19). However, there are limitations to these optogenetic strategies, particularly that they require overexpression of an artificial form of STIM1 (or a STIM1–Orai1 chimera) and cannot be used to control the native activity of endogenously expressed STIM–Orai complexes during physiologically relevant scenarios. In the present work, we address this issue with photopharmacology (20–22), a method reliant on small molecule ligands with biological activity that can be modulated with light. Our implementation uses the small molecule photoswitch azobenzene fused to pharmacologically useful analogs of the CRAC channel inhibitor 2-aminoethoxydiphenyl borate (2-APB), thereby imbuing the resulting compounds with light-dependent activity (Fig. 1*C*). We

Significance

Calcium release–activated calcium (CRAC) channels play key roles in the regulation of cellular signaling, transcription, and migration. Here, we describe the design, chemical synthesis, and characterization of photoswitchable channel inhibitors that can be switched on and off depending on the wavelength of light used. We use the compounds to induce light-dependent modulation of channel activity and downstream gene expression in human immune cells. We further expand the usage of the compounds to control seeding of cancer cells in target tissue and regulation of response to noxious stimuli in vivo in mice.

Author affiliations: [a]Department of Biochemistry, Technion Integrated Cancer Center, Ruth and Bruce Rappaport Faculty of Medicine, Technion Israel Institute of Technology, Haifa 31096 Israel; [b]Department of Chemistry, University of Connecticut, Storrs, CT 06269; [c]Department of Cell Biology and Cancer Science, Technion Integrated Cancer Center, Ruth and Bruce Rappaport Faculty of Medicine, Technion Israel Institute of Technology, Haifa 31096, Israel; [d]Department of Medical Neurobiology, Institute for Medical Research Israel–Canada, The Hebrew University Hadassah Medical School, Jerusalem 91120, Israel; and [e]The Edmond and Lily Safra Center for Brain Sciences, The Hebrew University of Jerusalem, Jerusalem 9190401, Israel

Author contributions: N.E., S.L., A.M.B., Y.S., M.A.K., and R.P. designed research; R.U., A.S., E.Z., H.A.C., J.H., N.E., S.L., M.A.K., and R.P. performed research; A.S., Y.S., M.A.K., and R.P. contributed new reagents/analytic tools; R.U., A.S., E.Z., H.A.C., J.H., N.E., S.L., A.M.B., M.A.K., and R.P. analyzed data; and A.M.B., M.A.K., and R.P. wrote the paper.

The authors declare no competing interest.

This article is a PNAS Direct Submission.

[1]R.U., A.S., and E.Z. contributed equally to this work.

[2]To whom correspondence may be addressed. Email: Michael.kienzler@uconn.edu or Razpalty@technion.ac.il.

This article contains supporting information online at http://www.pnas.org/lookup/suppl/doi:10.1073/pnas.2118160119/-/DCSupplemental.

Published March 21, 2022.

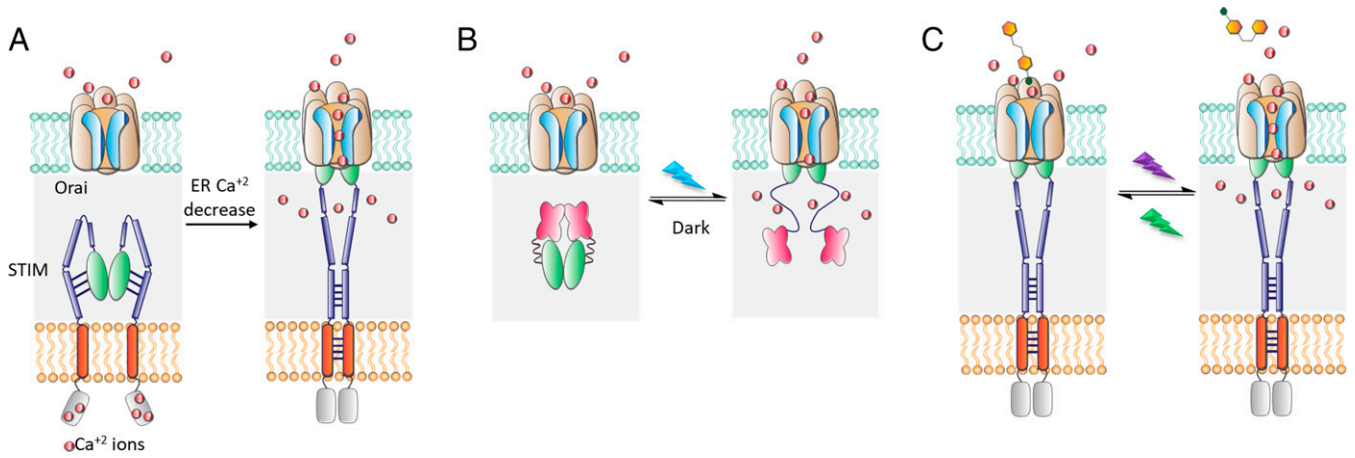

Fig. 1. CRAC channel activation and photocontrol. (*A*) Depletion of ER Ca^{+2} causes STIM aggregation and activation of CRAC channels by binding to Orai. (*B*) Opto-CRAC provides photocontrol of Ca^{+2}-dependent events through a fusion construct of the STIM1–Orai1-activating region (SOAR) domain and plant-derived photosensory light-activated voltage domain 2 (LOV2). (*C*) Use of the azobenzene-based photoswitch LOCI enables control of native CRAC channel activity using UV and visible light.

refer to these compounds as LOCIs (light-operated CRAC channel inhibitors) and have employed electrophysiological and imaging techniques to demonstrate that LOCIs control the activity of native CRAC channels in a light-dependent manner.

Results

Design, Synthesis, and Characterization of LOCIs. 2-APB has been shown to induce complex and contradictory effects on CRAC channels, namely current potentiation at low (~5 μM) concentrations and current inhibition at high concentrations (50 to 100 μM), which limits the utility of the compound (23, 24). Structure–activity relationship studies of 2-APB and its analogs (*SI Appendix*, Scheme S1*A*) provide key information: First, modifications to the ethoxyamine moiety have little effect, as this section of the molecule hydrolyzes readily under physiological conditions (25, 26) (*SI Appendix*, Scheme S1*B*). Second, the boron–oxygen core is essential for the potentiating effect; however, it is not required for inhibition (27). Finally, extended aromatic character and dimerization increases the efficiency of channel inhibition (28). Using this information, we reasoned that a straightforward azobenzene substitution would yield a set of azobenzene analog borinic and boronic acids (LOCI-1) and hydrolytically stable pinacol esters (LOCI-2) that could potentially modulate CRAC channel function in a light-dependent manner (Scheme 1). LOCI-2 was synthesized via Mills reaction from commercially available 4-aminophenylboronic acid pinacol ester and nitrosobenzene (*SI Appendix*, Scheme S2) (29). Removal of the hydrolysis-resistant pinacol ester in LOCI-2 to form the boronic acid LOCI-1 was performed via a transesterification process using methyl boronic acid and 5% trifluoroacetic acid (30). Investigation of the photoswitching properties of LOCI-1 showed that it behaves as a "regular" azobenzene (31) (Fig. 2*A*) with the *trans* isomer having ultraviolet/visible (UV/Vis) light absorption peaks at 329 nm (π-π*) and 440 nm (n-π*). LOCI-1 and LOCI-2 have nearly identical UV/Vis absorption spectra (*SI Appendix*, Fig. S1*A*). Repeated illumination (eight cycles) of LOCI-1 in a 1% dimethyl sulfoxide (DMSO) in phosphate-buffered saline (PBS) buffer proceeded without significant photofatigue (Fig. 2*B*). Using ^{1}H NMR spectroscopy, we observed that dark-adapted LOCI-1 is 94% *trans* isomer, while constant illumination at 365 nm until reaching a photostationary state (PSS_{365}) produced a 21:79 *trans:cis* ratio, and illumination at 520 nm (PSS_{520}) yielded a 70:30 *trans:cis* ratio (*SI Appendix*, Fig. S1*C*). Monitoring thermal relaxation of the *cis* isomer at 25 °C in 1% DMSO in PBS buffer revealed a half-life of 2.5 h (*SI Appendix*, Fig. S1*D*). Consumer-grade commercial light-emitting diodes (LEDs) (Sunlite LED) were sufficient to achieve photoswitching (Fig. 2 and *SI Appendix*, Fig. S1*B*), with all of the tested visible light LEDs having PSSs that are predominantly the *trans* isomer (*SI Appendix*, Fig. S1*B*). The LEDs were again used to obtain time-resolved UV/vis spectra of LOCI-1 (23 μM in 1% DMSO in PBS buffer) under continuous irradiation with 365 nm light (Fig. 2*C*) and 520 nm light (Fig. 2*D*) to their respective PSSs. Light intensity affects the time to reach the PSS at a given wavelength (Fig. 2 *E* and *F*). Using a powerful UV light source (100 W mercury arc lamp), a *trans* isomer solution of LOCI-1 can be driven to its predominantly *cis* PSS_{365} in under 1 min with high-intensity (35 mW/cm^2) light. We found that lower intensity (3.1 mW/cm^2) illumination still reaches the PSS in 5 min and is of sufficient power for further experiments. Should experimental parameters warrant it, there is precedent for azobenzene switches being driven to a majority *cis* PSS on a millisecond timescale with sufficiently intense laser light sources in the context of electrophysiology (32). Collectively, these experiments demonstrate that LOCI-1 behavior in an aqueous solution is dictated by illumination wavelength and power. Further, 365 nm light is widely available (in the form of LEDs or mercury arc lamps) and is satisfactory for driving the *trans* to *cis* photoisomerization of LOCI-1.

LOCI-1 and LOCI-2 control CRAC channel function in a light-dependent manner. To determine the effect of LOCI-1 and LOCI-2 on CRAC channels, we expressed STIM1 and Orai1 in HEK293 cells and employed the whole-cell configuration of the patch-clamp technique to directly measure Ca^{2+} entry by CRAC channels. To activate CRAC channels, the intracellular pipette solution contained thapsigargin, an endoplasmic/sarcoplasmic Ca^{2+} pump inhibitor (TG, 1 μM), and either of the Ca^{2+} chelating agents BAPTA [ethylene glycol-bis (1,2-bis(*o*-aminophenoxy)ethane-N,N,N′,N′-tetraacetic acid, 8 mM] or EGTA [ethylene glycol-bis(2-aminoethylether)-N,N,N′,N′-tetraacetic acid, 10 mM]. The CRAC current was inhibited by addition of either 2-APB (100 μM), LOCI-1 (10 μM), or LOCI-2 (10 μM). Illumination with 360 nm light restored current only in the presence of LOCI-1 or LOCI-2 but not in that of 2-APB (Fig. 3 *A* and *B*). These results show that LOCI-1 or LOCI-2 enable photosensitive control over CRAC currents.

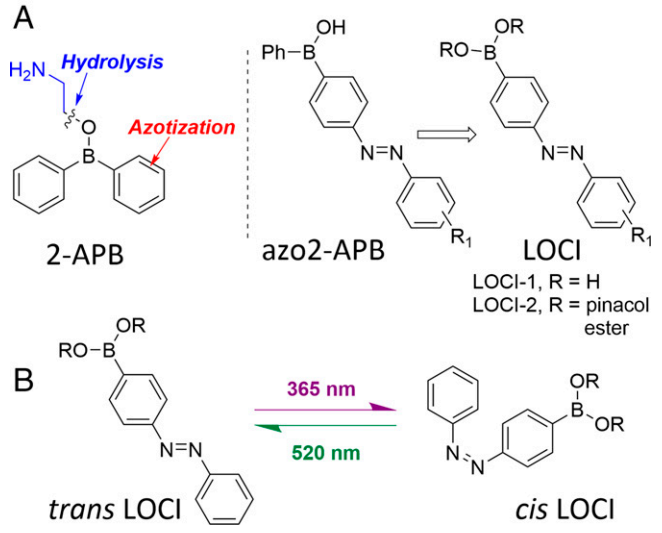

Scheme 1. 2-APB structure–activity relationships informed the design of LOCIs. (*A*) "Azotization" of 2-APB through intermediate LOCIs with either the free boronic acid (LOCI-1) or pinacol ester (LOCI-2). (*B*) *Trans* LOCI-1 can be efficiently isomerized to the *cis* isomer using UV light (365 nm) and switched back to the *trans* isomer using green light (520 nm).

Dose–response analysis showed that both LOCI-1 and LOCI-2 inhibit CRAC currents with a half maximal inhibitory concentration (IC_{50}) of 6.75 μM (Fig. 3 *C* and *D*, and *SI Appendix*, Fig. S2*A*), a value comparable to that of 2-APB (IC_{50} ~5 to 8 μM) (23, 33). Although both LOCI-1 and LOCI-2 exhibited strong current suppression, 360 nm light illumination fully restored current inhibition by LOCI-1 but only partially restored inhibition by LOCI-2 (Fig. 3*B*). We therefore selected LOCI-1 for further characterization. Consistent with its absorption peak near 330 nm in DMSO, action spectrum analysis showed that current induction was maximal at 360 nm light irradiation (Fig. 3*E*). Ca^{2+} imaging experiments further confirmed the effect of LOCI-1 on SOCE. HEK293 cells were incubated with extracellular solution containing 1 mM Ca^{2+} and either LOCI-1 (100 μM) or DMSO after TG was applied to deplete ER Ca^{2+} stores and activate SOCE. Imaging of intracellular Ca^{2+} levels under these conditions showed that SOCE was inhibited in the presence of LOCI-1 but not DMSO (*SI Appendix*, Fig. S2*B*). In line with these results, induction of SOCE by Ca^{2+} addback following ER Ca^{2+} depletion was attenuated in cells treated with LOCI-1 as compared to DMSO-treated cells (*SI Appendix*, Fig. S2*C*). We next used this experimental design to evaluate the spatial control over SOCE in cells (Fig. 3 *F* and *G*). Cells were treated with TG in the presence of LOCI-1, while only a fraction of the whole imaging area was illuminated with 365 nm light. Demonstrating the ability of LOCI-1 to allow spatial control over SOCE, cells localized within the 365-nm illuminated area showed robust SOCE, while cells localized outside this area did not (Fig. 3*G* and Movie S1). Taken together, results from Fig. 3 show that LOCI-1 enables optical control over CRAC channel activity in a precise spatial and temporal manner.

LOCI-1 selectively inhibits Orai1 and Orai2 channel activity. Having shown that LOCI-1 does not potentiate CRAC channel activity at low micromolar concentrations (Fig. 3*D* and *SI Appendix*, Fig. S2), we next asked whether the pharmacological profile of LOCI-1 further diverges from that of 2-APB. 2-APB has been shown to inhibit function of inositol trisphosphate receptor (InsP3R) (34) and several members of the transient receptor potential cation channels including TRPC6 (35), TRPC3 (36), and TRPV1 (37). Consistent with a marked

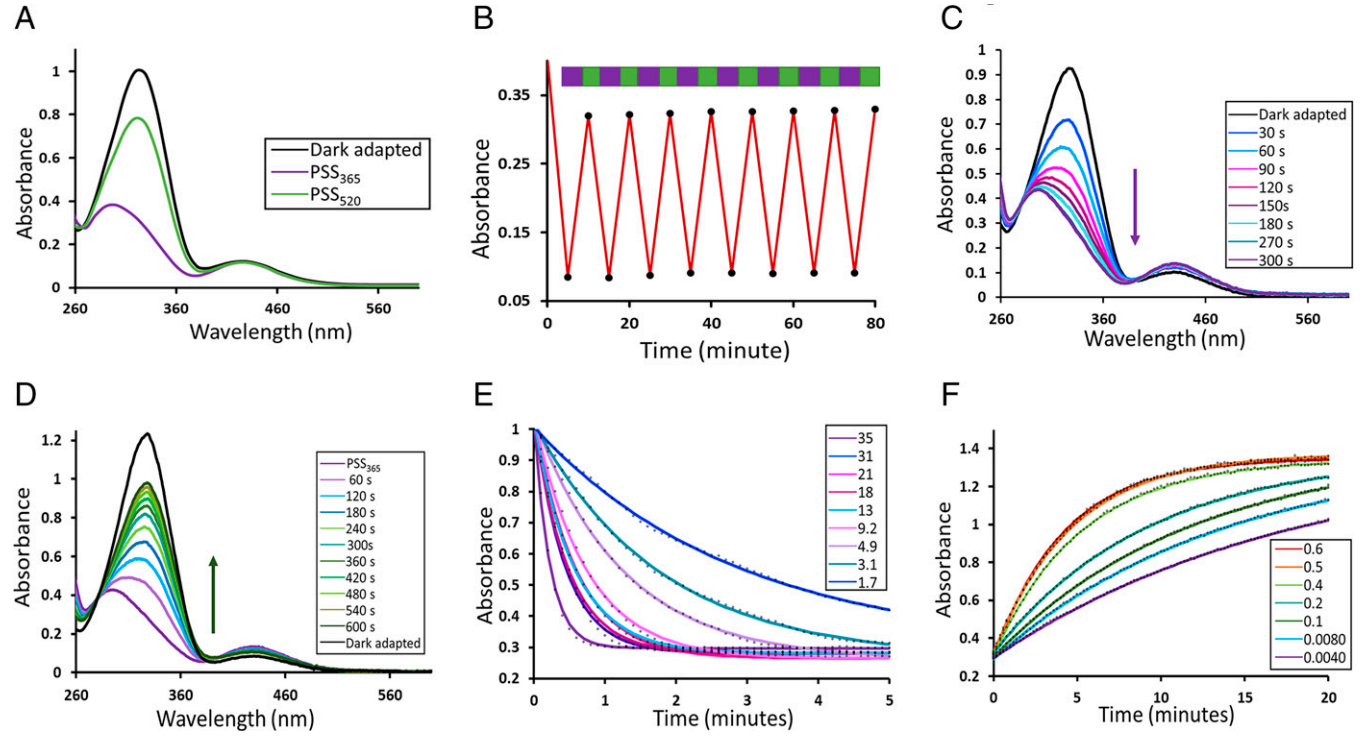

Fig. 2. Photochemical characterization of LOCI-1. (*A*) UV/Vis absorption spectra of LOCI-1 (22 μM) in DMSO, with dark-adapted (black), photostationary state with 365 nm LED illumination PSS_{365nm} (purple) and PSS_{520nm} (green) states when irradiated with UV and green light for 5 min, respectively. (*B*) Photostability of LOCI-1 (26 μM) in a 1% DMSO in PBS buffer solution. Absorbance changes recorded at 329 nm under alternating 5-min light illumination of 365 nm (purple) and 520 nm (green) for eight cycles. (*C* and *D*) Time resolved UV/Vis spectra of LOCI-1 (23 μM) during irradiation with 365 nm and 520 nm LEDs, respectively. (*E* and *F*) Absorbance of LOCI-1 (23 μM) monitored at 329 nm upon illumination with a high power 365-nm light source (Omnicure S1000 100 W mercury arc lamp) and a 520-nm LED at different irradiation powers, measured in mW/cm^2.

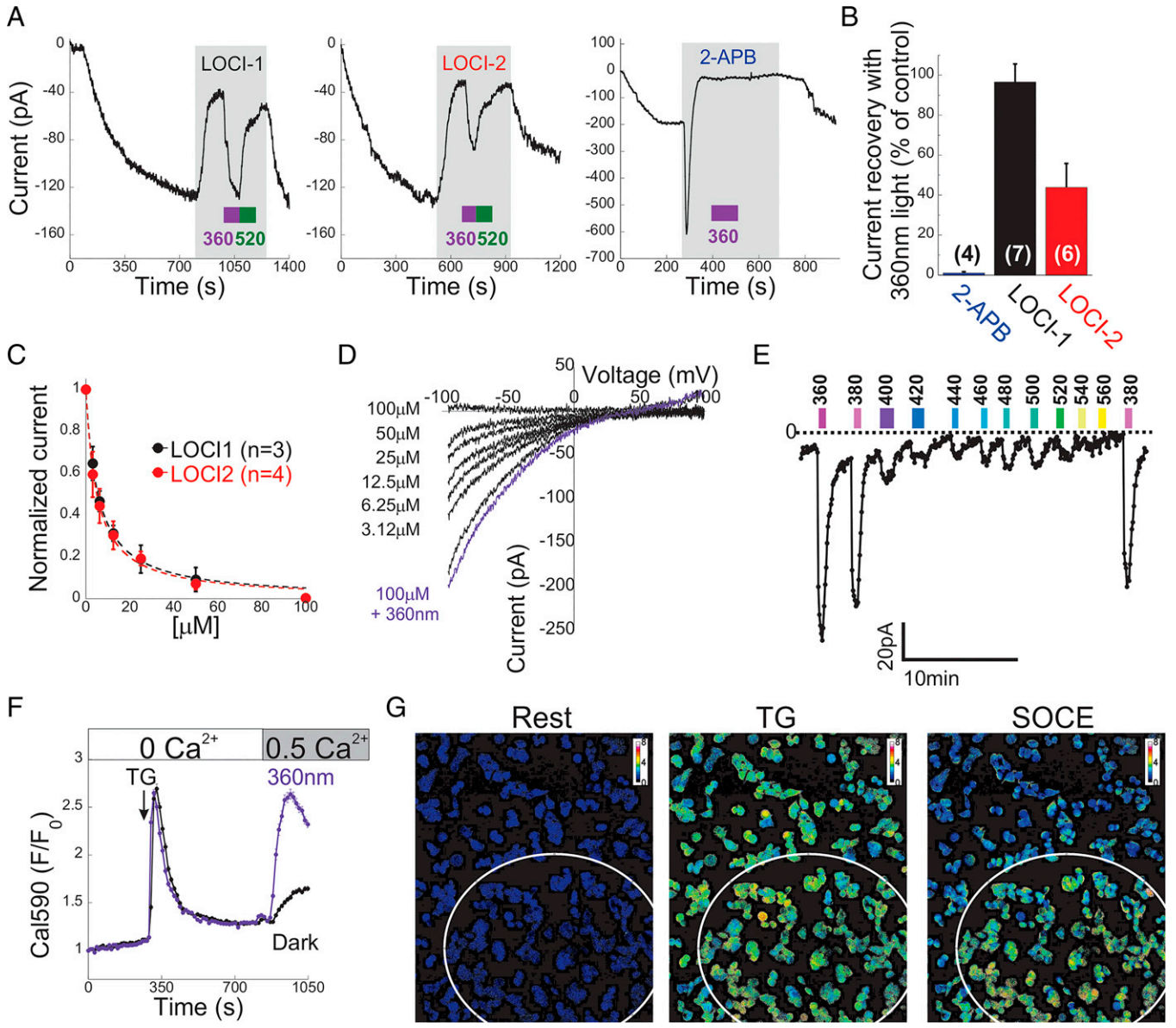

Fig. 3. LOCI-1 and LOCI-2 enable optical control over CRAC channel function. (*A* and *B*) A total of 20 mM BAPTA and 1 μM TG were included in the recording pipette solution to deplete ER Ca^{2+} and activate CRAC currents in HEK293 cells expressing STIM1 and Orai1. Cells were bathed in 10 mM Ca^{2+} and subsequently superfused (gray) with 10 mM Ca^{2+} external solution supplemented with LOCI-1 (10 μM), LOCI-2 (10 μM), or 2-APB (100 μM), as indicated. Either 360 nm or 520 nm light was shone at the indicated time points. (*B*) Bar graph showing the averaged fraction of current recovered by 360 nm light. Numbers within bars represent the number of cells in each analysis. (*C*) Dose-inhibition analysis for LOCI-1 (n = 3) and LOCI-2 (n = 4). K_i = 5.5 ± 0.26 μM for LOCI-1 and 4.96 ± 0.28 μM for LOCI-2. (*D*) Current–voltage (I-V) traces measured at the indicated concentration of LOCI-1 and during 360 nm illumination. (*E*) Modulation of CRAC currents by LOCI-1 by brief illumination of light at the indicated wavelengths. (*F* and *G*) LOCI-1 enables spatial control over SOCE in HEK293. Wild-type (WT) HEK293 were loaded with the Ca^{2+} indicator Cal-590, incubated with 100 μM LOCI-1, and addition of thapsigargin (400 nM, as indicated) was used to deplete ER luminal Ca^{2+} under zero extracellular Ca^{2+}. SOCE was subsequently activated upon superfusion with extracellular solution containing 0.5 mM Ca^{2+}. A subregion of cells (white circle) was illuminated with 365 nm light for 5 s before each frame) to locally photoswitch LOCI-1 to the noninhibiting *cis* conformation. (*F*) Time course of Cal-590 fluorescence from cells imaged without (dark, n = 85) or with (purple, n = 29) 365 nm illumination. (*G*) Images show the normalized Cal-590 fluorescence at time points 0 (rest), 330 (TG), and 960 (SOCE) seconds.

pharmacological change between LOCI-1 and 2-APB, LOCI-1 effectively suppressed SOCE but did not affect IP3-mediated Ca^{2+} release or TRPC3-, TRPC6-, or TRPV1-mediated Ca^{2+} influx (Fig. 4*A* and *SI Appendix*, Fig. S2). These results indicate that irrespective of its light sensitivity, LOCI-1 operates as a more straightforward and selective CRAC channel inhibitor than 2-APB. Further indicating that LOCI-1 exerts specific effects on SOCE, application of LOCI-1 to cells overexpressing NCX1 did not inhibit sodium–calcium exchange activity mediated by this transporter (Fig. 4*A*). We next investigated the effect of LOCI-1 on CRAC currents in cells coexpressing STIM1 together with either Orai2 or Orai3 channels. Dose–response analysis showed that Orai2 is sensitive to LOCI-1 (K_i = 15.5 ± 1.8 μM) (Fig. 4*B*). In contrast, LOCI-1 exhibited low affinity for Orai1 (K_i = 131 ± 24 μM) and produced only a small inhibitory effect on Orai3 activity with average inhibition of ∼35% in the presence of 100 μM LOCI-1. Next, we reconstituted the expression of each Orai isoform together with STIM1 in HEK293 cells with triple deletion of Orai1, Orai2, and Orai3 (Orai triple knockout [TKO] cells) and performed Ca^{2+} imaging experiments to test the effect of LOCI-1 on Ca^{2+} entry mediated by each Orai isoform. The effect of LOCI-1 on SOCE mediated by each individual Orai isoform was determined using the same experimental design as

in Fig. 3*F*. Results from these Ca^{2+} imaging experiments were consistent with results from current recordings and showed that LOCI-1 strongly inhibits SOCE mediated by Orai1 or Orai2 but not by Orai3 (Fig. 4 *C* and *D*). Furthermore, 365 nm light restored SOCE or current in Orai1- or Orai2-expressing cells but had only a minor effect in Orai3-expressing cells (Fig. 4 *C* and *D* and *SI Appendix*, Fig. S4 *A* and *B*). Since 2-APB is known to activate a STIM1-independent and nonselective Orai3 conductance (38), we investigated whether LOCI-1 exerts a similar effect on Orai3 channels. Fig. 5*A* shows that when either Orai1 or Orai3 was expressed alone, application of 100 μM LOCI-1 with or without 360 nm light illumination did not induce a notable current change. As expected, subsequent application of 2-APB, however, induced strong currents in Orai3 (127.2 ± 19.7 pA/pF, $n = 3$) but not in Orai1 (1.89 ± 0.1 pA/pF, $n = 3$)-expressing cells (Fig. 5*A*). Taken together, the above results indicate that while both LOCI-1 and 2-APB inhibit CRAC channel function, the two compounds exhibit very different pharmacological properties.

LOCI-1 inhibits Orai1 through an extracellular-facing site localized close to the channel pore. In light of the distinct pharmacological profiles of LOCI-1 and 2-APB, we next investigated the mechanism of action of LOCI-1. Since 2-APB has been shown to affect clustering of STIM1 at ER–PM junctions, we initially examined whether LOCI-1 interferes with this activity of STIM1 (39). In further divergence from 2-APB, after ER Ca^{2+} depletion with TG, LOCI-1 did not affect the clustering of STIM1 in puncta at ER–PM junctions (Fig. 5*B* and *SI Appendix*, Fig. S3). Fig. 5*B* further shows that LOCI-1 also does not inhibit coclustering of STIM1 and Orai1 at ER–PM junctions under these conditions. These results indicate that LOCI-1 does not inhibit CRAC channel function by preventing puncta formation by STIM1 or interaction between STIM1 and Orai1. We next asked whether LOCI-1 exerts a direct effect on Orai1 independently of STIM1. To this end, we analyzed the effect of LOCI-1 on Orai1 channels harboring either the pore mutation V102A or the TM4 mutation P245L, which constitutively opens the channel in the absence of STIM1 (40, 41). As shown in Fig. 5*C*, while application of 10 μM LOCI-1 had a negligible effect on the Orai1 V102A current, it strongly inhibited the Orai1 P245L current and this inhibition was partially recovered by 360 nm illumination (Fig. 5 *D* and *E*). Analysis of Ca^{2+} flux by Orai1 P245L in STIM double knockout (DKO) cells yielded similar results (*SI Appendix*, Fig. S3 *C–E*) confirming that LOCI-1 modulates Orai1 function independently of STIM proteins. Taken together, these findings

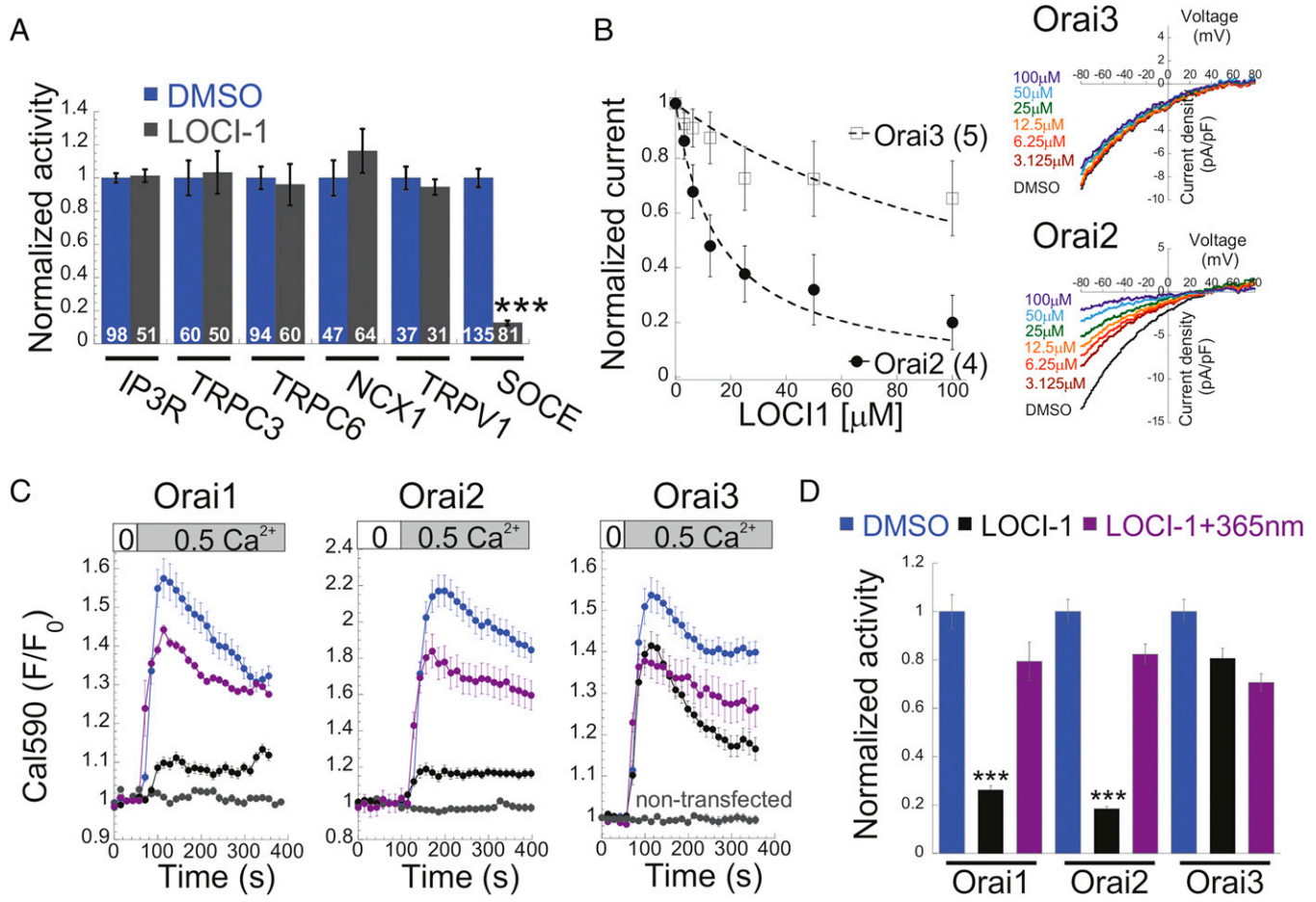

Fig. 4. LOCI-1 selectively inhibits channel activity of Orai1 and Orai2. (*A*) Quantification of IP3-mediated intracellular Ca^{2+} release, Na^+/Ca^{2+} exchange, or Ca^{2+} entry via SOCE, TRPV1, TRPC3, or TRPC6 channels in cells treated with DMSO or LOCI-1 (100 μM). The change in intracellular Ca^{2+} levels following activation of each Ca^{2+} transport mechanism in the presence of LOCI-1 was normalized to the change in control cells (DMSO). Additional information for this analysis is shown in *SI Appendix*, Fig. S2. (*B*) Dose-inhibition analysis for LOCI-1 was performed in cells expressing STIM1 together with Orai2 (K_i = 15.5 ± 1.8 μM) or Orai3 (K_i = 131 ± 24 μM). Panels show the dose-dependent inhibition (*Left*) and corresponding I-V plots (*Right*) of Orai2 or Orai3 currents by the indicted concentration of LOCI-1. (*C*) Orai TKO HEK293 cells expressing STIM1 together with either Orai1, Orai2, or Orai3 were loaded with Cal-590 and incubated in Ca^{2+}-free solution containing 1 μM TG for 10 min. Plots show the time course of Cal-590 fluorescence before and after superfusion with 0.5 mM Ca^{2+} containing solution without or with 365 nm illumination. (*D*) Quantification of SOCE mediated by the indicated Orai isoform in the presence of DMSO (control) or LOCI-1 (100 μM) in the dark or under 365 nm light. n = 21 to 185 cells in each group, ***$P < 0.001$.

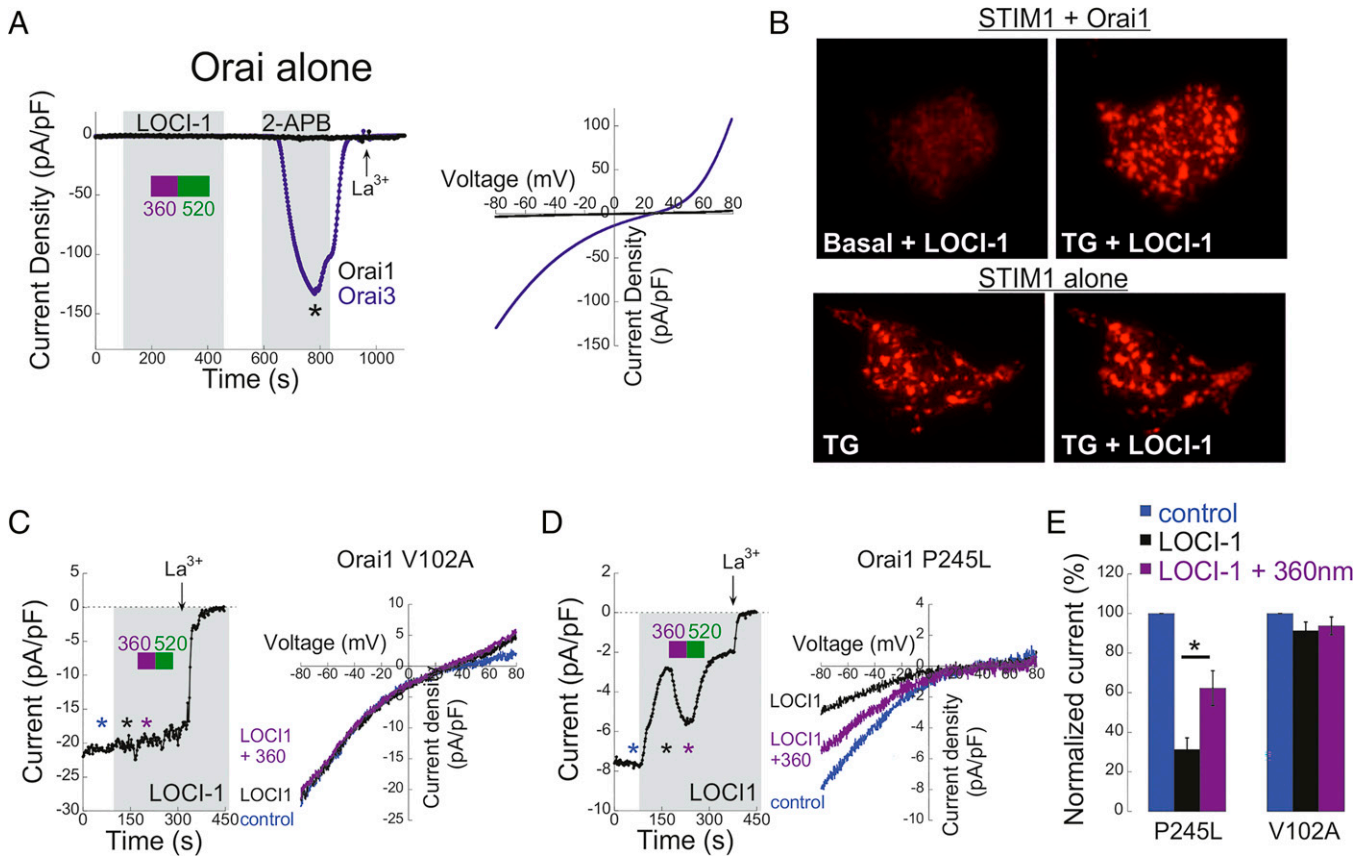

Fig. 5. LOCI-1 inhibits CRAC channel activity through an extracellular site proximal to the channel pore. (*A*, *Left*) Time course of current recording from HEK293 cells expressing either Orai1 (black trace) or Orai3 (blue trace) following superfusion with extracellular solution containing 10 mM Ca^{2+} with or without 100 μM LOCI-1 or 100 μM 2-APB. (*A*, *Right*) I-V plots of 2-APB induced current measured at the indicated time point (asterisk). (*B*, *Upper*) A cell expressing Orai1-EGFP and STIM1-mCherry was incubated in zero Ca^{2+} extracellular solution containing 100 μM LOCI-1 and the cell's membrane was imaged using TIRFM before and 10 min after addition of 400 nM thapsigargin. (*B*, *Lower*) A cell expressing STIM1-mCherry alone was incubated in zero Ca^{2+} extracellular solution containing 400 nM thapsigargin for 10 min to allow for accumulation of STIM1 at ER–PM junctions. A total of 100 μM LOCI-1 was subsequently added and the cell's membrane was imaged using TIRFM before and 20 min after addition of LOCI-1. (*C* and *D*) Time course (*Left*) and I-V plots (*Right*) of currents from cells expressing the V102A Orai1 mutant (*C*) or P245L Orai1 mutant (*D*). Cells were superfused with an extracellular solution containing 10 mM Ca^{2+} with or without 10 μM LOCI-1 or 10 μM La^{3+}, as indicated. During recordings, cells were kept in the dark or illuminated with the indicated wavelengths of light. Pipette solution contained 20 mM BAPTA. (*E*) Bar graph shows the average normalized currents of Orai1 V102A ($n = 4$) or Orai1 P245L ($n = 5$) before and after application of 10 mM LOCI-1 under dark or following illumination with 360 nm light. $^*P < 0.05$, $^{***}P < 0.001$.

indicate LOCI-1 inhibits Orai1 directly and suggest that destabilization of the channel pore by the V102A mutation interferes with this inhibition. The activating mutation of V102 in Orai1 dilates the channel pore (40) and hence may affect the inhibitory function of LOCI-1 by modulating a site on Orai1 that is found at or proximal to the pore. Because the amino acid sequences of Orai1 and Orai3 are identical at the pore-lining TM1 region, but not across the intracellular N-terminal tail region or across the extracellular loop connecting TM1 to TM2 where the degree of similarity decreases, we asked whether either of these regions is necessary for channel inhibition by LOCI-1. Accessibility analysis revealed that LOCI-1 controls channel activity only when applied extracellularly (Fig. 6*A*) and failed to do so when infused into the cytosol via the patch pipette (Fig. 6 *B* and *C*). This finding suggests that LOCI-1 affects Orai1 through an extracellular-facing site. To further explore the role of the TM1–TM2 extracellular loop region in LOCI-1–mediated channel inhibition, we created chimeric Orai1–Orai3 (O1–O3) constructs in which we exchanged the N-terminal regions ending at the TM1–TM2 loop of the two Orai isoforms (Fig. 6*D*). When coexpressed with STIM1, either one of these chimeric channels exhibited a typical store-operated CRAC current; however, while application of 10 μM LOCI-1 had only a small and inconsistent effect on current in cells expressing the O3N–O1C channel (Fig. 6 *E* and *G* and *SI Appendix*, Fig. S4*G*), it strongly inhibited the current in cells expressing the reciprocal chimeric O1N–O3C channel and 360 nm light partially restored the current (Fig. 6 *F* and *G* and *SI Appendix*, Fig. S4*F*). Results from analysis of SOCE in Orai TKO HEK293 cells coexpressing STIM1 together with either one of the two chimeric Orai1–Orai3 channels were consistent with the effect of LOCI-1 on currents (*SI Appendix*, Fig. S5). Since the region spanning TM2 to TM3 in Orai3 has been shown to be critical for the effect of 2-APB (42), we also created Orai1–Orai3 chimeric constructs in which this region was exchanged in the two Orai isoforms. Analysis of SOCE in cells expressing these constructs showed that replacement of the TM2 to TM3 regions in Orai1 and Orai3 does not affect the light-operated control of LOCI-1 on channel activity (*SI Appendix*, Fig. S5). Taken together with results from accessibility analysis, these findings indicate that the N-terminal region of Orai1 ending at the TM1–TM2 loop is necessary and sufficient for light-dependent modulation of channel activity by LOCI-1 and suggest that the binding site for LOCI-1 may localize to a site on the extracellular loop connecting TM1 and TM2 in Orai1.

LOCI-1 Enables Optical Control of Ca^{2+}-Dependent Gene Expression in T Lymphocytes. In T lymphocytes, CRAC channels constitute the main route for Ca^{2+} influx and are essential for

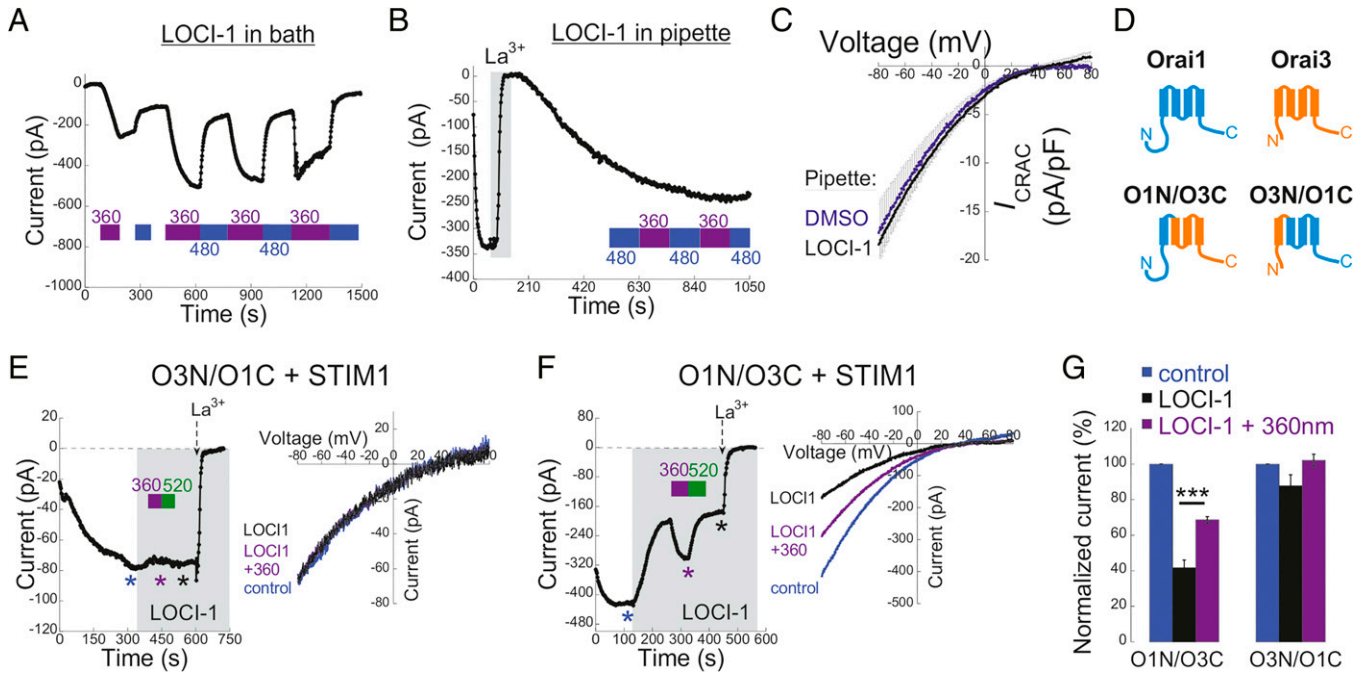

Fig. 6. LOCI-1 inhibits CRAC channel activity through an extracellular site proximal to the channel pore. (*A–C*) Current recording from cells expressing Orai1 and STIM1. LOCI-1 was constantly present either at 100 μM in bath solution (*A*) or at 0.5 mM in the pipette solution (*B*), and 480 or 360 nm light was illuminated at the indicated time points. (*C*) Averaged I-V plots recorded from cells expressing STIM1 and Orai1. LOCI-1 (0.5 mM, $n = 3$) or DMSO ($n = 4$) was added to pipette solution, as indicated. (*D*) Illustration of the Orai1, Orai3, and Orai1–Orai3 chimeric constructs used in *E–G*. (*E* and *F*) Time course (*Left*) and I-V plots (*Right*) of currents from cells expressing STIM1 together with the O3N/O1C construct (*E*) or O1N/O3C construct (*F*). I-V plots correspond to currents at time points indicated by blue, purple, and black asterisks. Cells were superfused with an extracellular solution containing 10 mM Ca^{2+} with or without 10 μM LOCI-1 or 10 μM La^{3+}, as indicated. During recordings, cells were kept in the dark or illuminated with the indicated wavelengths of light. Pipette solution contained 20 mM BAPTA and 1 μM TG. (*G*) Bar graph shows the average normalized currents of the O3N/O1C construct ($n = 6$) or O1N/O3C ($n = 4$) before and after application of 10 μM LOCI-1 under dark or following illumination with 360 nm light. ***$P < 0.001$.

T cell function and adaptive immunity (43). Ca^{2+} flux through CRAC channels elevates intracellular Ca^{2+} levels and stimulates the Ca^{2+}–calcineurin–NFAT signaling pathway, which in turn regulates the expression of a large number of T cell activation–related genes (44–46 and Fig. 7*D*). We therefore investigated whether LOCI-1 is able to control signaling through the Ca^{2+}–calcineurin–NFAT pathway in Jurkat T cells, a well-established model for human T cell biology (47). Dose–response analysis showed that the native CRAC current is sensitive to LOCI-1 (Fig. 7*A*). However, the affinity ($K_i = 22.7 \pm 1.7$ μM) and the efficacy (~74 ± 5%) of inhibition were similar to those recorded in HEK293 cells coexpressing STIM1–Orai2 and somewhat reduced as compared to those in STIM1–Orai1 cells (Fig. 7*A* and *SI Appendix*, Fig. S6*A*). These changes may reflect a dominant effect of Orai2 on LOCI-1 sensitivity in Jurkat T cells; alternatively, considering the externally facing binding site for LOCI-1 on Orai1 (Fig. 6), these changes may arise from changes in cell-type–specific glycosylation of Orai1 (48). Similar to the effect of LOCI-1 on the STIM1–Orai1 or STIM1–Orai2 current in HEK293 cells, irradiation with 360 nm light restored the fraction of inhibited current (Fig. 7*B* and *SI Appendix*, Fig. S6*B*). In agreement with the effect of LOCI-1 on the native CRAC current, imaging of intracellular Ca^{2+} levels in T cells treated with TG (1 μM) and either LOCI-1 or 2-APB showed that periodic illumination by 360 nm light is followed by transient intracellular Ca^{2+} rises (Fig. 7*B*) in the presence of LOCI-1 but not 2-APB (100 μM), indicating that only LOCI-1 enables light-dependent Ca^{2+} influx. Next, we monitored Ca^{2+}-dependent gene expression in T cells (Fig. 7*C*). Jurkat T lymphocytes containing an NFAT-inducible luciferase reporter gene (JNL cells) were treated with TG, PMA (phorbol 12-myristate 13-acetate), and either DMSO or LOCI-1 (100 μM) for 16 h and luciferase expression was subsequently monitored to assess NFAT transcription. Initial experiments using LOCI-1 kept strictly in the dark showed a concentration-dependent inhibition (*SI Appendix*, Fig. S6*B*). To expose cells to the *cis* conformation of LOCI-1 over an extended period of time, the cell chamber was positioned under a wide 365-nm illumination area (3.1 cm^2) and the entire chamber region was exposed to 10 s of 365 nm light every 30 min during the initial 60-min period. Because the concentration of *cis* LOCI-1 thermally decays back to *trans* LOCI-1 slowly (half-life of 2.5 h at 25 °C) (*SI Appendix*, Fig. S1*D*), this illumination setup ensures that depletion of *trans* LOCI-1 persists between UV pulses. As shown in Fig. 7*E*, in the dark LOCI-1 inhibited NFAT transcription by more than 80% and two pulses of 365 nm light were sufficient to fully restore transcription to control levels. These results show that LOCI-1 effectively controls Ca^{2+}-regulated gene expression in T lymphocytes in a light-dependent manner and suggest that it may serve as a powerful tool for light-guided immune modulation.

LOCI enables optical modulation of seeding of cancer cells at metastatic sites. Having shown that LOCI-1 enables optical control over CRAC channel function in vitro, we next extended our analysis to animal models. A growing body of evidence indicates an important role for SOCE in pathological conditions, including cancer (49, 50) and pain (51–53). We therefore tested whether LOCI-1 can be used in vivo to modulate seeding of cancer cells at metastatic sites or acute pain responses to noxious stimuli. Owing to its critical roles in tumor cell migration and adhesion, SOCE is important for metastasis of cancer cells (49, 54). Metastasis is a multistep process that includes dissemination of cancer cells from the primary tumor; their intravasation to the blood or lymphatic systems; survival

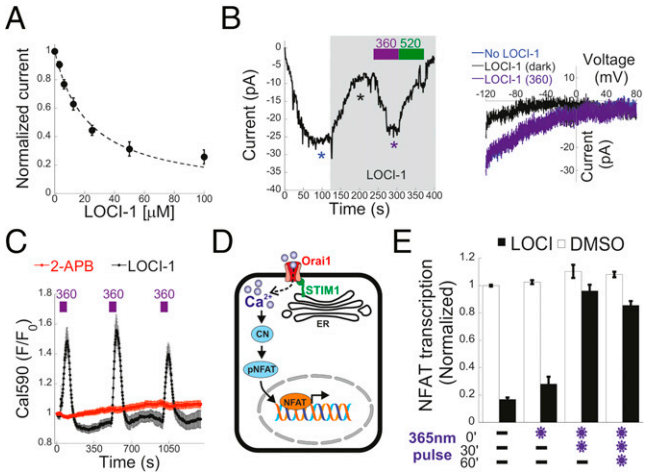

Fig. 7. LOCI-1 enables light-dependent control of gene expression through the Ca^{2+}-dependent NFAT pathway in T lymphocytes. (*A*) Dose-inhibition analysis of native CRAC current by LOCI-1 in Jurkat cells. K_i = 22.7 ± 1.7 μM, *n* = 5. (*B, Left*) Time course of CRAC current in Jurkat T cells following addition of 20 mM Ca^{2+} with and without 100 μM LOCI-1 and during periodic illumination of 360 nm and 520 nm light, as indicated. (*B, Right*) I-V plots of currents before and after application of 100 μM LOCI-1 in the dark and under illumination with 360 nm light, as indicated by asterisk. (*C*) Time course of intracellular Ca^{2+} traces in individual Jurkat T cells. Cells were loaded with the Ca^{2+} indicator Cal-590, incubated with TG (1 μM) and 100 μM of either LOCI-1 or 2-APB and briefly exposed to 360 nm light at the indicated time points. (*D*) Scheme for Ca^{2+}–calcineurin–NFAT signaling pathway in T lymphocytes. (*E*) NFAT-dependent gene expression experiment in JNL cells. Cells were stimulated with PMA (10 ng/mL) and Tg (1 μM) and incubated for 16 h in the presence of vehicle (DMSO) or LOCI-1 (100 μM). Cells were kept in the dark (dash) or exposed to a brief 10-s illumination of 365 nm light at time points 0, 30, and 60 min (purple star), as indicated. NFAT transcriptional activity was determined with a luminescence-based assay (*Materials and Methods*).

in the circulation; and extravasation, seeding, and proliferation at the metastatic site (55). To test whether LOCI-1 can be used to modulate tumor cell seeding at metastatic sites we used a pulmonary metastatic assay (PuMA) (Fig. 8*A*). In this assay, murine breast cancer cells stably expressing GFP (EMT6-GFP) were injected into mice through the tail vein and allowed to adhere and infiltrate into the lungs for 20 min. Lungs were subsequently removed and cultured ex vivo for 7 d after which the number of metastatic colonies was evaluated. Subsequently, lung slices were prepared as single cell suspensions and the percentage of GFP-positive cells in lung tissue was evaluated by flow cytometry. As expected, control cells treated with DMSO produced a large number of visible colonies of GFP-positive cancer cells that accounted for ∼1.4% of all cells in the lung tissue (Fig. 8 *B* and *C*). In contrast, cells treated with LOCI-1 produced significantly fewer metastatic colonies and the relative number of cancer cells in lungs was more than twofold lower (∼0.65%), suggesting that LOCI-1 successfully inhibits metastatic cell seeding. Importantly, in cells treated with LOCI-1 and 365 nm illumination, both the number of metastatic colonies and the relative amount of cancer cells in lungs (∼1.3%) were significantly elevated, indicating that LOCI-1 enables light-dependent control of a key step during metastasis of cancer cells.

LOCI enables optical modulation of nocifensive behavior in mice. We next examined whether LOCI-mediated optical modulation of CRAC channels can alter responses to noxious stimuli. Accumulating evidence suggests that the CRAC channel plays an important role in the processing of noxious information by the central nervous system (CNS) (51–53, 56); however, the role of the channels in the detection and transmission of noxious stimuli by primary afferent nociceptive neurons remains poorly understood. We examined the effect of LOCI-mediated optical modulation of CRAC channels on the nocifensive behavior triggered by capsaicin-induced activation of nociceptive terminals innervating mouse cornea (57, 58). To control for a direct effect of LOCI-1 on the capsaicin-sensitive receptor-channel TRPV1, we performed Ca^{2+} imaging experiments on HEK293 STIM DKO cells expressing TRPV1 and found that TRPV1 activity is unchanged in the presence of either the *cis* or *trans* confirmations of LOCI-1 (*SI Appendix*, Figs. S2 and S7). Capsaicin-sensitive, TRPV1-expressing nociceptive terminals originate from somata situated in the trigeminal ganglion (TG) (Fig. 8*D*), constituting the main population of neurons that innervate the cornea (59). We found that acutely dissociated cultured mouse TG neurons exhibited a robust SOCE, which was inhibited when cells were incubated with LOCI-1 (100 μM). Consistent with results from HEK293 and T cells, illumination with 360 nm light restored SOCE in LOCI-1–treated neurons, indicating that TG neurons have significant SOCE that can be modulated by LOCI-1 in a light-dependent manner. Given the selective effect of LOCI-1 on CRAC in TG neurons but not TRPV1 channels, and the relative transparency of the cornea to UV light, we exploited LOCI-1 to investigate the role of SOCE in capsaicin-induced nocifensive behavior in freely moving mice. To this end, capsaicin was administered topically to the mouse eye and the typical repetitive forelimb eye wiping behavior was measured to evaluate the degree of the nocifensive response (58) (Fig. 8*E*). The occurrence of eye wiping in normal conditions was initially determined in vehicle-treated control mice. The response in control mice was similar to that in mice treated with LOCI-1 alone or in mice exposed to 365 nm light, indicating that when applied alone, neither LOCI-1 nor 365 nm light elicits an appreciable nocifensive behavior (Fig. 8*F*). As expected, mice treated with capsaicin exhibited a significant increase in the number of eye wipings, compared to the basal response of control mice (Fig. 8*F*). Remarkably, mice cotreated with both LOCI-1 and capsaicin exhibited significantly lower responses, which were similar to the responses in vehicle-treated mice. These results suggest that CRAC channels in nociceptive terminals play an essential role in the detection of noxious stimuli. Notably, the inhibitory effect of LOCI-1 was fully reversed by a pulse of 365 nm light (Fig. 8*F*). Taken together, these results suggest that by modulating SOCE in corneal nociceptive nerve endings, photoswitching of LOCI-1 affects acute pain.

Discussion

We present LOCI-1, a small molecule photoswitch formed by combining azobenzene and the phenylborate core of the CRAC channel modulator 2-APB, which enables effective and reversible optical control over Ca^{2+} influx through native CRAC channels. LOCI-1 undergoes reversible isomerization after absorption of UV or visible light. In its *trans* photoisomer, LOCI-1 interacts with an externally accessible site on the Orai1 channel and inhibits channel activation by STIM1; 365 nm of light-induced isomerization to the *cis* conformation removes this inhibition. Our results show that unlike 2-APB, LOCI-1 regulates Ca^{2+} entry mediated by Orai1 and Orai2 in a straightforward dose-dependent manner and does not potentiate the STIM1-dependent Orai1 current or the STIM1-independent Orai3 current. In further divergence from 2-APB, which inhibits STIM1-dependent Orai3 currents by about ∼70% (60), LOCI-1 exerts only a minor inhibitory effect on

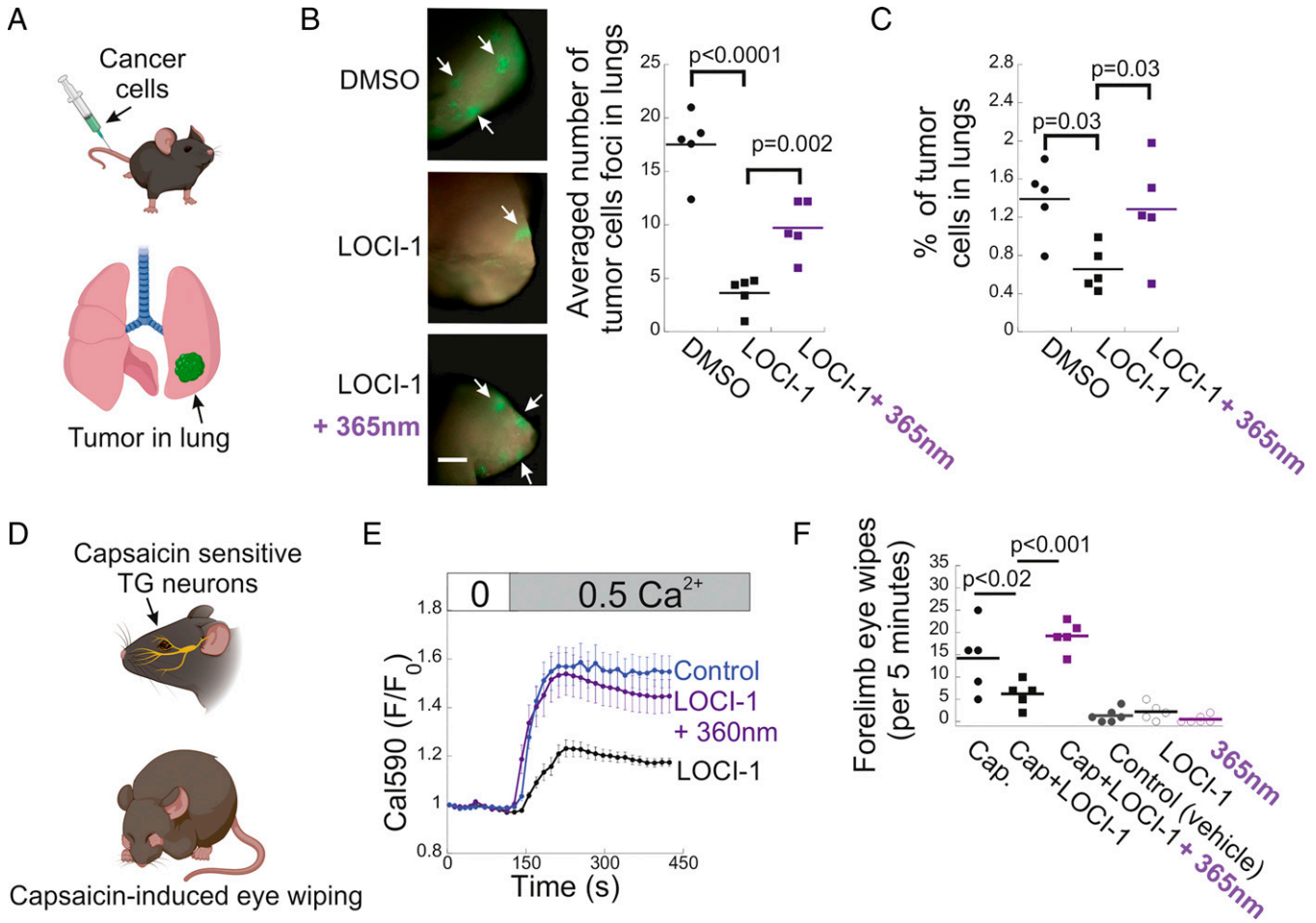

Fig. 8. LOCI-1 enables light-dependent control of metastatic cell seeding and nocifensive responses in mice. (*A*) Illustration of the pulmonary metastatic assay. (*B*, *Left*) Representative images of GFP fluorescence with brightfield overlay of cultured lung slices excised from mice treated with DMSO, LOCI-1 (200 μM), or LOCI-1 (200 μM) together with illumination of 365 nm light, as indicated. (*B*, *Right*) Summary of the average number of GFP-positive colonies from three different lung slices per mice (five mice per group) for each treatment. (*C*) The percentage of GFP-positive cells out of the total lung cells from each mouse was evaluated by flow cytometry. (Scale bar, 200 μm.) (*D*) Illustration of innervation of trigeminal neurons (*Upper* cartoon) and the eye wiping behavior analyzed in *F* after installation of capsaicin to the eye. (*E*) Acutely dissociated cultured trigeminal ganglion neurons were loaded with Cal-590 and incubated in Ca^{2+}-free solution containing 1 μM thapsigargin with (n = 179) or without (n = 139) 100 μM LOCI-1 for 10 min. Plots show the time course of Cal-590 fluorescence before and after induction of SOCE by superfusion with a 0.5 mM Ca^{2+}-containing solution without or with 360 nm illumination (n = 71). (*F*) Means and individual values of the numbers of eye wiping following corneal installation of either vehicle (0.1% ethanol in SES), capsaicin (Cap, 1 μM), LOCI-1 (100 μM), or a combination of both capsaicin and LOCI-1. Two additional groups consisting of mock-treated or capsaicin and LOCI-1–treated mice were subjected to a pulse of 365 nm light. Recording of freely moving mice started 5 min after each of the indicated treatments and the number of forelimb eye wipes for each mouse was measured during an additional 5-min period.

STIM1-induced Orai3 currents. These properties deviate from the complex effects on Orai1 and Orai3 channel activity induced by 2-APB and highlight the utility of LOCI-1 as a tool for probing channel function under physiologically relevant conditions. In this regard, we find that LOCI-1 successfully modulates a number of biological processes that are highly regulated by CRAC channel function. First, we show that LOCI-1 successfully blocks the native CRAC current and Ca^{2+}-dependent gene expression in T lymphocytes in a light-dependent manner. As Ca^{2+} flux through CRAC channels regulates multiple aspects of mammalian T cell function, LOCI-1 could serve as a tool for controlling lymphocyte signaling, for example, as a model therapeutic agent for cell-based immunotherapy approaches. Such a model can potentially address the pressing need for switchable immunomodulators that are able to tune down hyperimmune activity associated with life-threatening adverse effects (61, 62). In a second application of LOCI-1, we find it is able to control metastatic seeding of breast cancer cells. While the involvement of CRAC channels in cancer metastasis is well documented throughout the literature (50, 63), whether CRAC channels play distinct roles at different stages of this multistep process remains poorly understood. The ability of LOCI-1 to control metastatic seeding of cancer cells in a light-dependent manner offers a powerful tool that can be used in future studies to elucidate the precise role of Ca^{2+} entry through CRAC channels during metastatic spreading of cancer cells. Our findings that LOCI-1 efficiently blocks the spread of EMT6 cells is consistent with the established role of Orai1, but not Orai3, in metastasis of estrogen receptor negative breast cancer cells (50, 64, 65). Hence, in light of the important contribution of Orai3 to SOCE in breast cancer cells expressing estrogen receptors (64, 65), the ability of LOCI-1 to discriminate between Ca^{2+} entry mediated by Orai1 and Orai3 represents another important advantage of the usage of LOCI-1 in cancer research. In a third application of LOCI-1, we show its ability to modulate SOCE in TG neurons and to affect pain-associated responses in a light-dependent manner in mice. We note that while CRAC channels have been shown to play a key role in shaping neuronal excitability of both dorsal horn and dorsal root neurons (51, 66) as well as in the modulation of

behavioral response to painful nociceptive stimuli (51, 52), whether the channel is important for detection, transmission, or modulation of noxious stimuli at the peripheral sensory site remained poorly understood. Our finding that local application of LOCI-1 to the mouse eye suppresses capsaicin-induced pain responses in a light-dependent manner suggests that CRAC channels play a particularly important role in shaping the noxious signal at the peripheral sensory site. Taken together, with the lack of direct effect of LOCI-1 on TRPV1 function, these findings further establish LOCI-1 as a highly advantageous tool for future interrogations of the specific role of SOCE in signal transmission in capsaicin-sensitive neuronal afferents. A noteworthy potential caveat of LOCI-1, however, is that the boronic acid is anticipated to interact with a variety of biomolecules that may be found on the surface of cells, particularly sugars (67). While our findings indicate that LOCI-1 also does not cross-react with NCX1, InsP3R, or either TRPC3 or TRPC6 channels, other yet-to-be identified, off-target effects of LOCI-1 remain possible. Nonetheless, in view of its effective light-operated control on CRAC channel function, we believe that LOCI-1 may also establish the basis for a tethered CRAC channel photoswitch in future studies.

During the preparation of this manuscript, Yang et al. (68) reported the synthesis of piCRAC, an azopyrazole-derived photoswitchable CRAC channel inhibitor. Notably, in addition to their distinct chemical structures, the functional properties of LOCI-1 and piCRAC vary in several ways. First, each photoswitchable molecule induces inhibition of CRAC channel activity in opposite conformations—the *trans* conformation for LOCI-1 and the *cis* conformation for piCRAC. Second, both dynamics and extent of light-induced CRAC channel regulation by each compound are distinct. Acute administration of LOCI-1 completely inhibits the CRAC current with an IC_{50} of ~6.75 μM, and 365 nm light fully recovers inhibition within 1 to 2 min. Conversely, following chronic administration of piCRAC, illumination at 365 nm enables partial suppression of CRAC channel activity with relatively high affinity (IC_{50} of ~0.5 μM); however, recovery from inhibition is slow and incomplete (~57% recovery after 15 min) (68). Finally, LOCI-1 can be used to discriminate between Orai1- and Orai3-mediated Ca^{2+} entry in cells. While it is presently unknown whether piCRAC exerts an isoform-specific inhibition of Orai channels, such an effect appears unlikely, given that the Orai3 current has been shown to be sensitive to the GSK7975A and GSK5503A (69) compounds that are structurally similar to the piCRAC parent compound GSK5498A (68). Hence, while both LOCI-1 and piCRAC enable optical control over CRAC channel function, the two photoswitches work in distinct and complementary ways.

In summary, we have developed an effective CRAC channel photoswitch that allows optical control over channel activity in a dynamic and reversible manner. Given the exceptional ability of LOCI-1 to shape the activity of native CRAC channels at different spatial and temporal scales, we believe that this tool and its derivatives will contribute significantly to future interrogation of a variety of cellular processes that are regulated by CRAC channel activity.

Materials and Methods

Photoswitchability and Thermal Stability of LOCI-1. All UV spectra were recorded using either a SpectraMax i3x from Molecular Devices or Vernier UV/Vis spectrophotometer (VSP-UV). Photoswitching experiments were performed using LEDs (PAR 16 colored series bulbs from Sunlite, 2.8 W, 120 V, 240 lumens, and Sunlite A19/LED/2 W/120 V 100 lm [365, 460, 520, and 593 nm], and McDOER Blacklight Flashlight UV 100 LED 18 W, 391 nm). The power density of the LEDs was determined using a power meter (General UV513AB UVA/B light meter or Thorlabs PM100D) held 1 cm from the source: 365 nm (8.7 mW/cm^2), 391 nm (0.34 mW/cm^2), 460 nm (12.6 mW/cm^2), 520 nm (8.8 mW/cm^2), and 593 nm (1.5 mW/cm^2). Further experiments using 365 nm (UV) and 520 nm (green) light were run with the light source stationed at a distance of 1 cm from the cuvette containing the sample. Some experiments (Fig. 2*E*) relied on a high-intensity UV light source (Omnicure S1000 100 W mercury arc lamp).

Thermal relaxation (*cis*→*trans* isomerization) for LOCI-1 was recorded at room temperature (25 °C) in triplicates using a Vernier UV/Vis spectrophotometer. An initial UV/Vis spectra of *trans* LOCI-1 in the dark was recorded. The dark adapted *trans* LOCI-1 was then irradiated with 365 nm UV light for 5 min and absorbance at $\lambda = 329$ nm of the irradiated sample was recorded in triplicates over 30 h. Absorbance was plotted as a function of time. Thermal half-life was calculated using $t_{1/2} = 0.693/k$. SE of measurement (SEm) of the triplicate data was calculated using the equation: $SEm = S\sqrt{1 - r_x}$, where S is the SD and r_x is reliability of the test. The Solver add-on in Microsoft Excel was used to find a line fit using the GRG nonlinear engine using the equation $Abs(t) = Abs_{BI} + (Abs_{365nm} - Abs_{BI}) * \exp(-kt)$, where k is the rate constant, t is time, Abs_{BI} is absorbance before illumination, and Abs_{365nm} is absorbance at PSS_{365}. The variables Abs_{BI}, Abs_{365nm}, and k were used as free parameters in the fit.

Total Internal Reflection Fluorescence Microscopy. Total internal reflection fluorescence microscopy (TIRFM) was performed as described previously (70) using an inverted Olympus IX83 microscope combined with a cellTIRF-4Line system (405/488/561/640 nm lasers) and equipped with a back-illuminated scientific complementary metal oxide semiconductor (sCMOS) camera (Prime 95B, Photometrics). Fluorescence was collected by 100× (numerical aperture [N.A.] 1.49) objective.

Fluorescence Measurements of Intracellular Ca^{2+}Ions. To load cells with Cal-590 (AAT Bioquest), cells were incubated for 60 min in Ringer's solution containing 5 μM of the Ca^{2+} indicator. To record cytosolic Ca^{2+} levels, cells were excited by illumination at 560 nm delivered by monochromator (Visitron). Illumination was further filtered by 560/40 excitation filter, projected through a 585-long pass beamsplitter, and emission was collected with a 630/75-nm filter. Periodic illumination with 360 nm (16.1 mW/cm^2) or 365 nm (18.5 mW/cm^2) light during intracellular Ca^{2+} imaging was done by 360/365 nm illumination (for photoswitching LOCI-1) together with brief (50 to 100 ms) alternations to 560 nm (59 mW/cm^2) illumination (for imaging Cal-590 fluorescence). Images were acquired every 3 or 10 s with a back-illuminated sCMOS camera (Prime 95B, Photometrics). In each experiment, traces from 10 to 97 cells were recorded and the averaged response from all cells was plotted with KaleidaGraph.

NFAT-Dependent Luciferase Assay. Jurkat NFAT-P/Luciferase (JNL) cells were stimulated for 16 to 18 h as indicated. During the first 90 min of stimulation, cells were either kept in the dark or illuminated for 10 s with 365 nm light (16 mW/cm^2) every 30 min. Treatments were done in triplicates of 40×10^3 cells/well in 96-well plates. Luminescence was measured with a Tecan Infinite 200 Pro plate reader using the Steady-Glo luciferase assay system (Promega). All the data were normalized against the control group.

Pulmonary Metastasis Assay. A PuMA was performed as previously described (71, 72). Briefly, 1 h prior to tail vein injection, EMT6-GFP^+ cells were treated with either 1% DMSO or LOCI-1 (200 μM) without or together with illumination at 365 nm (16 mW/cm^2) for 10 s at time points 0, 30, and 60 min. Subsequently, the cells were washed in PBS and then injected into the tail vein of 8-wk-old BALB/c mice (5×10^4 cells per mouse). Considering that the total mouse blood volume is ~2 mL, the effective concentration of LOCI-1 after injection is expected to be ~20 μM. Twenty minutes later, the mice were anesthetized, and lungs were perfused with PBS. Next, the trachea was cannulated with a 21-G intravenous catheter and attached to a gravity perfusion apparatus. The lungs were filled with heated agarose medium solution containing M-199 media (×2), 7.5% sodium bicarbonate, 0.2 μg/mL hydrocortisone, 2.0 μg/mL bovine insulin, 200 U/mL penicillin/streptomycin, and 1% agarose at a ratio of 1:1, agarose to medium (wt/vol). The lungs were removed and placed in cold PBS.

Transverse 1- to 2-mm-thick serial sections were sliced with a scalpel. Each section was incubated on Matrigel-covered plates for 7 d at 37 °C in 5% Dulbecco's modified Eagle medium. The lung slices were analyzed for GFP^+ cells using an Olympus MVX109 fluorescence stereomicroscope. Subsequently, the lungs were prepared as a single cell suspension and the percentage of GFP^+ cells was quantified by flow cytometry, as previously described (73). Statistical significance was determined with ANOVA using Student–Newman–Keuls multiple comparison analysis; $P < 0.05$ was considered significant. All data are shown as mean ± SEM. The use of animals and experimental protocol was approved by the Animal Care and Use Committee at Technion (ethic no. IL0890716).

Nocifensive Behavioral Tests. Capsaicin-induced nocifensive behavior was analyzed using the forelimb eye wiping test as described previously (57). Briefly, five to six male C57BL/6JOLAHSD mice (3 to 4 wk old) were used in each experimental group. Prior to all experiments, mice were handled and habituated to the experimental procedures for 2 d. The behavioral assays were performed in an open-top, clear, standard mouse cage. The mice were habituated to the setup for 10 min prior to each assay.

Each assay consisted of the installation of a 10-μL drop containing either 1 μM capsaicin, vehicle (0.1% ethanol in standard external solution (SES)), 100 μM LOCI-1, or 1 μM capsaicin together with 100 μM LOCI-1 to the right eye of the mouse. Five minutes after installation, the eye wiping behavior was recorded for 5 min and analyzed post hoc. Photoswitching of LOCI-1 was done by directing 365 nm light (16 mW/cm^2) to the right eye of the mouse at a distance of 3 cm for 60 s and analysis started 5 min after the illumination pulse. The eye wiping test was also performed following 365 nm illumination alone in order to test for light-induced irritation. The use of animals and experimental protocol was approved by the animal ethics committees of the Hebrew University of Jerusalem (MD18-15608).

LOCI Synthesis. Details for LOCI synthesis are provided in *SI Appendix*.

Cell Culture and Electrophysiology. Details for cell culture, plasmid transfection, and electrophysiology are provided in *SI Appendix*.

Data Availability. All study data are included in the article and/or supporting information.

ACKNOWLEDGMENTS. This work was supported by grants from the NSF (Grant 2116412 to M.A.K.), the Israeli Science Foundation (Grant 1048/18 to R.P. and Grant 1470/17 to A.M.B.), the Sessile and Seymour Alpert Chair in Pain Research (A.M.B.), the US–Israel Binational Science Foundation (Grant 2019657 to R.P.), and the Rappaport Research Institute (2018 Thematic Grant to R.P. and Y.S.).

1. M. Prakriya, R. S. Lewis, Store-operated calcium channels. *Physiol. Rev.* **95**, 1383–1436 (2015).
2. M. Hoth, R. Penner, Depletion of intracellular calcium stores activates a calcium current in mast cells. *Nature* **355**, 353–356 (1992).
3. R. S. Lewis, M. D. Cahalan, Mitogen-induced oscillations of cytosolic Ca2+ and transmembrane Ca2+ current in human leukemic T cells. *Cell Regul.* **1**, 99–112 (1989).
4. L. Zhang, M. A. McCloskey, Immunoglobulin E receptor-activated calcium conductance in rat mast cells. *J. Physiol.* **483**, 59–66 (1995).
5. J. Roos *et al.*, STIM1, an essential and conserved component of store-operated Ca2+ channel function. *J. Cell Biol.* **169**, 435–445 (2005).
6. S. L. Zhang *et al.*, STIM1 is a Ca2+ sensor that activates CRAC channels and migrates from the Ca2+ store to the plasma membrane. *Nature* **437**, 902–905 (2005).
7. J. Liou *et al.*, STIM is a Ca2+ sensor essential for Ca2+-store-depletion-triggered Ca2+ influx. *Curr. Biol.* **15**, 1235–1241 (2005).
8. M. Prakriya *et al.*, Orai1 is an essential pore subunit of the CRAC channel. *Nature* **443**, 230–233 (2006).
9. M. Vig *et al.*, CRACM1 is a plasma membrane protein essential for store-operated Ca2+ entry. *Science* **312**, 1220–1223 (2006).
10. S. Feske *et al.*, A mutation in Orai1 causes immune deficiency by abrogating CRAC channel function. *Nature* **441**, 179–185 (2006).
11. S. L. Zhang *et al.*, Genome-wide RNAi screen of Ca(2+) influx identifies genes that regulate Ca(2+) release-activated Ca(2+) channel activity. *Proc. Natl. Acad. Sci. U.S.A.* **103**, 9357–9362 (2006).
12. A. V. Yeromin *et al.*, Molecular identification of the CRAC channel by altered ion selectivity in a mutant of Orai. *Nature* **443**, 226–229 (2006).
13. C. Peinelt *et al.*, Amplification of CRAC current by STIM1 and CRACM1 (Orai1). *Nat. Cell Biol.* **8**, 771–773 (2006).
14. R. S. Lacruz, S. Feske, Diseases caused by mutations in ORAI1 and STIM1. *Ann. N. Y. Acad. Sci.* **1356**, 45–79 (2015).
15. L. He *et al.*, Near-infrared photoactivatable control of Ca(2+) signaling and optogenetic immunomodulation. *eLife* **4**, e10024 (2015).
16. T. Ishii *et al.*, Light generation of intracellular Ca(2+) signals by a genetically encoded protein BACCS. *Nat. Commun.* **6**, 1–15 (2015).
17. T. Kyung *et al.*, Optogenetic control of endogenous Ca(2+) channels in vivo. *Nat. Biotechnol.* **33**, 1092–1096 (2015).
18. E. Pham, E. Mills, K. Truong, A synthetic photoactivated protein to generate local or global Ca(2+) signals. *Chem. Biol.* **18**, 880–890 (2011).
19. S. Kim *et al.*, Non-invasive optical control of endogenous Ca^{2+} channels in awake mice. *Nat. Commun.* **11**, 1–10 (2020).
20. K. Hüll, J. Morstein, D. Trauner, In vivo photopharmacology. *Chem. Rev.* **118**, 10710–10747 (2018).
21. M. M. Lerch, M. J. Hansen, G. M. van Dam, W. Szymanski, B. L. Feringa, Emerging targets in photopharmacology. *Angew. Chem. Int. Ed. Engl.* **55**, 10978–10999 (2016).
22. W. A. Velema, W. Szymanski, B. L. Feringa, Photopharmacology: Beyond proof of principle. *J. Am. Chem. Soc.* **136**, 2178–2191 (2014).
23. C. Peinelt, A. Lis, A. Beck, A. Fleig, R. Penner, 2-Aminoethoxydiphenyl borate directly facilitates and indirectly inhibits STIM1-dependent gating of CRAC channels. *J. Physiol.* **586**, 3061–3073 (2008).
24. M. Prakriya, R. S. Lewis, Potentiation and inhibition of Ca(2+) release-activated Ca(2+) channels by 2-aminoethyldiphenyl borate (2-APB) occurs independently of IP(3) receptors. *J. Physiol.* **536**, 3–19 (2001).
25. A. Hofer *et al.*, Design, synthesis and pharmacological characterization of analogs of 2-aminoethyl diphenylborinate (2-APB), a known store-operated calcium channel blocker, for inhibition of TRPV6-mediated calcium transport. *Bioorg. Med. Chem.* **21**, 3202–3213 (2013).
26. M. G. Chudzinski, Y. Chi, M. S. Taylor, Borinic acids: A neglected class of organoboron compounds for recognition of diols in aqueous solution. *Aust. J. Chem.* **64**, 1466–1469 (2011).
27. O. Dellis, P. Mercier, C. Chomienne, The boron-oxygen core of borinate esters is responsible for the store-operated calcium entry potentiation ability. *BMC Pharmacol.* **11**, 1 (2011).
28. A. Djillani, O. Nüße, O. Dellis, Characterization of novel store-operated calcium entry effectors. *Biochim. Biophys. Acta* **1843**, 2341–2347 (2014).
29. J. H. Harvey, B. K. Butler, D. Trauner, Functionalized azobenzenes through cross-coupling with organotrifluoroborates. *Tetrahedron Lett.* **48**, 1661–1664 (2007).
30. S. P. A. Hinkes, C. D. P. Klein, Virtues of volatility: A facile transesterification approach to boronic acids. *Org. Lett.* **21**, 3048–3052 (2019).
31. H. Rau, Spectroscopic properties of organic azo compounds. *Angew. Chem. Int. Ed. Engl.* **12**, 224–235 (1973).
32. A. Reiner, E. Y. Isacoff, Tethered ligands reveal glutamate receptor desensitization depends on subunit occupancy. *Nat. Chem. Biol.* **10**, 273–280 (2014).
33. J. Goto *et al.*, Two novel 2-aminoethyl diphenylborinate (2-APB) analogues differentially activate and inhibit store-operated Ca(2+) entry via STIM proteins. *Cell Calcium* **47**, 1–10 (2010).
34. H. T. Ma *et al.*, Requirement of the inositol trisphosphate receptor for activation of store-operated Ca2+ channels. *Science* **287**, 1647–1651 (2000).
35. S.-Z. Xu *et al.*, Block of TRPC5 channels by 2-aminoethoxydiphenyl borate: A differential, extracellular and voltage-dependent effect. *Br. J. Pharmacol.* **145**, 405–414 (2005).
36. J.-P. Lievremont, G. S. Bird, J. W. Putney, Jr, Mechanism of inhibition of TRPC cation channels by 2-aminoethoxydiphenylborane. *Mol. Pharmacol.* **68**, 758–762 (2005).
37. H.-Z. Hu *et al.*, 2-aminoethoxydiphenyl borate is a common activator of TRPV1, TRPV2, and TRPV3. *J. Biol. Chem.* **279**, 35741–35748 (2004).
38. A. Lis *et al.*, CRACM1, CRACM2, and CRACM3 are store-operated Ca2+ channels with distinct functional properties. *Curr. Biol.* **17**, 794–800 (2007).
39. W. I. DeHaven, J. T. Smyth, R. R. Boyles, G. S. Bird, J. W. Putney, Jr, Complex actions of 2-aminoethyldiphenyl borate on store-operated calcium entry. *J. Biol. Chem.* **283**, 19265–19273 (2008).
40. B. A. McNally, A. Somasundaram, M. Yamashita, M. Prakriya, Gated regulation of CRAC channel ion selectivity by STIM1. *Nature* **482**, 241–245 (2012).
41. R. Palty, C. Stanley, E. Y. Isacoff, Critical role for Orai1 C-terminal domain and TM4 in CRAC channel gating. *Cell Res.* **25**, 963–980 (2015).
42. S. L. Zhang *et al.*, Store-dependent and -independent modes regulating Ca2+ release-activated Ca2+ channel activity of human Orai1 and Orai3. *J. Biol. Chem.* **283**, 17662–17671 (2008).
43. M. Trebak, J.-P. Kinet, Calcium signalling in T cells. *Nat. Rev. Immunol.* **19**, 154–169 (2019).
44. P. G. Hogan, L. Chen, J. Nardone, A. Rao, Transcriptional regulation by calcium, calcineurin, and NFAT. *Genes Dev.* **17**, 2205–2232 (2003).
45. F. Macián *et al.*, Transcriptional mechanisms underlying lymphocyte tolerance. *Cell* **109**, 719–731 (2002).
46. R. S. Lewis, Calcium signaling mechanisms in T lymphocytes. *Annu. Rev. Immunol.* **19**, 497–521 (2001).
47. M. Montano, "2 - Model systems" in *Translational Biology in Medicine*, *Woodhead Publishing Series in Biomedicine*, M. Montano, Ed. (Woodhead Publishing, 2014), pp. 9–33.
48. K. Dörr *et al.*, Cell type-specific glycosylation of Orai1 modulates store-operated Ca2+ entry. *Sci. Signal.* **9**, ra25 (2016).
49. A. S. Hammad, K. Machaca, Store operated calcium entry in cell migration and cancer metastasis. *Cells* **10**, 1246 (2021).
50. S. Yang, J. J. Zhang, X.-Y. Huang, Orai1 and STIM1 are critical for breast tumor cell migration and metastasis. *Cancer Cell* **15**, 124–134 (2009).
51. Y. Dou *et al.*, Orai1 plays a crucial role in central sensitization by modulating neuronal excitability. *J. Neurosci.* **38**, 887–900 (2018).
52. J. Xia *et al.*, Orai1 is a crucial downstream partner of group I metabotropic glutamate receptor signaling in dorsal horn neurons. *Pain* 10.1097/j.pain.0000000000002396. (2021).
53. Z. Qi *et al.*, The central analgesic mechanism of YM-58483 in attenuating neuropathic pain in rats. *Cell. Mol. Neurobiol.* **36**, 1035–1043 (2016).
54. I. Jardin, J. A. Rosado, STIM and calcium channel complexes in cancer. *Biochim. Biophys. Acta* **1863** (6 Pt B), 1418–1426 (2016).
55. D. R. Welch, D. R. Hurst, Defining the hallmarks of metastasis. *Cancer Res.* **79**, 3011–3027 (2019).
56. R. Gao *et al.*, Potent analgesic effects of a store-operated calcium channel inhibitor. *Pain* **154**, 2034–2044 (2013).
57. R. H. Goldstein *et al.*, Location and plasticity of the sodium spike initiation zone in nociceptive terminals in vivo. *Neuron* **102**, 801–812.e5 (2019).
58. C. Belmonte, M. C. Acosta, J. Gallar, Neural basis of sensation in intact and injured corneas. *Exp. Eye Res.* **78**, 513–525 (2004).
59. A. Alamri, R. Bron, J. A. Brock, J. J. Ivanusic, Transient receptor potential cation channel subfamily V member 1 expressing corneal sensory neurons can be subdivided into at least three subpopulations. *Front. Neuroanat.* **9**, 71 (2015).

60. M. Yamashita, A. Somasundaram, M. Prakriya, Competitive modulation of Ca2+ release-activated Ca2+ channel gating by STIM1 and 2-aminoethyldiphenyl borate. *J. Biol. Chem.* **286**, 9429–9442 (2011).
61. L. A. Johnson, C. H. June, Driving gene-engineered T cell immunotherapy of cancer. *Cell Res.* **27**, 38–58 (2017).
62. R. A. Morgan *et al.*, Case report of a serious adverse event following the administration of T cells transduced with a chimeric antigen receptor recognizing ERBB2. *Mol. Ther.* **18**, 843–851 (2010).
63. A. Vashisht, M. Trebak, R. K. Motiani, STIM and Orai proteins as novel targets for cancer therapy. A review in the theme: Cell and molecular processes in cancer metastasis. *Am. J. Physiol. Cell Physiol.* **309**, C457–C469 (2015).
64. R. K. Motiani, I. F. Abdullaev, M. Trebak, A novel native store-operated calcium channel encoded by Orai3: Selective requirement of Orai3 versus Orai1 in estrogen receptor-positive versus estrogen receptor-negative breast cancer cells. *J. Biol. Chem.* **285**, 19173–19183 (2010).
65. R. K. Motiani *et al.*, Orai3 is an estrogen receptor α-regulated Ca^{2+} channel that promotes tumorigenesis. *FASEB J.* **27**, 63–75 (2013).
66. D. Wei, Y. Mei, J. Xia, H. Hu, Orai1 and Orai3 mediate store-operated calcium entry contributing to neuronal excitability in dorsal root ganglion neurons. *Front. Cell. Neurosci.* **11**, 400 (2017).
67. T. D. James, M. D. Phillips, S. Shinkai, *Boronic Acids in Saccharide Recognition* (RSC Publishing, 2006). https://doi.org/10.1039/9781847557612.
68. X. Yang *et al.*, Optical control of CRAC channels using photoswitchable azopy-razoles. *J. Am. Chem. Soc.* **142**, 9460–9470 (2020).
69. I. Derler *et al.*, The action of selective CRAC channel blockers is affected by the Orai pore geometry. *Cell Calcium* **53**, 139–151 (2013).
70. E. Zomot, H. Achildiev Cohen, I. Dagan, R. Militsin, R. Palty, Bidirectional regulation of calcium release-activated calcium (CRAC) channel by SARAF. *J. Cell Biol.* **220**, e202104007 (2021).
71. A. Mendoza *et al.*, Modeling metastasis biology and therapy in real time in the mouse lung. *J. Clin. Invest.* **120**, 2979–2988 (2010).
72. C. Rachman-Tzemah *et al.*, Blocking surgically induced lysyl oxidase activity reduces the risk of lung metastases. *Cell Rep.* **19**, 774–784 (2017).
73. M. Timaner, O. Beyar-Katz, Y. Shaked, Analysis of the stromal cellular components of the solid tumor microenvironment using flow cytometry. *Curr. Protoc. Cell. Biol.* **70**, 19.18.1–19.18.12 (2016).